

**Magic conditions for multiple rotational states of bialkali molecules in optical lattices**Q. Guan<sup>1</sup>, Simon L. Cornish<sup>2</sup>, and S. Kotochigova<sup>1</sup><sup>1</sup>*Department of Physics, Temple University, Philadelphia, Pennsylvania 19122, USA*<sup>2</sup>*Joint Quantum Centre (JQC) Durham-Newcastle, Department of Physics, Durham University, South Road, Durham DH1 3LE, United Kingdom*

(Received 16 January 2021; accepted 19 March 2021; published 7 April 2021)

We investigate magic-wavelength trapping of ultracold bialkali molecules in the vicinity of weak optical transitions from the vibrational ground state of the  $X^1\Sigma^+$  potential to low-lying rovibrational states of the  $b^3\Pi_0$  potential, focusing our discussion on the  $^{87}\text{Rb}^{133}\text{Cs}$  molecule in a magnetic field of  $B = 181$  G. We show that a frequency window exists between two nearest-neighbor vibrational poles in the dynamic polarizability where the trapping potential is “near magic” for multiple rotational states simultaneously. We show that the addition of a modest DC electric field of  $E = 0.13$  kV/cm leads to an exact magic-wavelength trap for the lowest three rotational states at an angular-frequency detuning of  $\Delta_{v'=0} = 2\pi \times 218.22$  GHz from the  $X^1\Sigma^+(v=0, J=0) \rightarrow b^3\Pi_0(v'=0, J=1)$  transition. We derive a set of analytical criteria that must be fulfilled to ensure the existence of such magic frequency windows and present an analytic expression for the position of the frequency window in terms of a set of experimentally measurable parameters. These results should inform future experiments requiring long coherence times on multiple rotational transitions in ultracold polar molecules.

DOI: [10.1103/PhysRevA.103.043311](https://doi.org/10.1103/PhysRevA.103.043311)**I. INTRODUCTION**

Ultracold polar molecules present a wealth of opportunities in quantum science and technology [1]. Proposed applications span the fields of precision measurement and metrology [2–8], quantum-state resolved chemistry [9–13], dipolar quantum matter [14–19], quantum simulation [20–25], and quantum information processing [26–32]. Recent experimental progress on the production of ultracold molecules by association [33–43] and direct laser cooling [44–49] has brought many of these applications within reach.

In the realm of quantum simulation and computation, the rotational structure of ultracold molecules provides a rich basis of long-lived states in which to encode pseudospins or quantum information. Owing to the permanent molecular-frame electric dipole moment, the rotational states can be conveniently manipulated with microwave fields, as already demonstrated in a number of settings [50–55]. Moreover, laboratory-frame dipole moments can be engineered using applied electric fields or superpositions of rotational states. The resulting long-range interaction between molecules can be exploited to realize model Hamiltonians in quantum magnetism [20,21,24,56–58] and two-qubit gates for quantum information processing [26–32]. To generate useful interaction strengths necessitates intermolecular distances below a micrometre. This is most readily achieved using optical potentials, either in the form of an optical lattice [59,60] or an array of optical tweezers [61,62].

For diatomic molecules, such as ground-state bialkali molecules [33–43], the dynamic polarizability along the molecular axis ( $\alpha_{\parallel}$ ) is, in general, different from that perpen-

dicular to it ( $\alpha_{\perp}$ ). For light polarized at an angle  $\theta$  to the molecular axis, this leads to a dynamic polarizability in the body-fixed frame given by

$$\alpha(\theta) = \alpha^{(0)} + \alpha^{(2)}P_2(\cos(\theta)), \quad (1)$$

where  $\alpha^{(0)} = \frac{1}{3}(\alpha_{\parallel} + 2\alpha_{\perp})$  and  $\alpha^{(2)} = \frac{2}{3}(\alpha_{\parallel} - \alpha_{\perp})$  are the isotropic and anisotropic components of the polarizability tensor, respectively.  $\alpha_{\parallel}$  and  $\alpha_{\perp}$  result from a sum over all allowed molecular transitions for the component of the dipole operator parallel or perpendicular to the molecular axis, respectively, and are smooth functions of wavelength in the regime where the frequency of the trapping laser is far detuned from any rovibronic transitions [63–65]. In the laboratory frame, the dynamic polarizability can be thought of as the spatial average of  $\alpha(\theta)$ . Although  $\alpha^{(0)}$  is the same for all rotational states,  $\alpha^{(2)}$  strongly mixes states with different rotational projections in excited rotational states. It follows that for molecules confined in an optical potential, the anisotropic polarizability leads to rotational transition frequencies that are strongly dependent on the intensity and polarization of the trapping light. The concomitant state-dependent light shifts make it highly challenging to achieve rotational coherence times that are sufficiently long to be sensitive to the  $\sim$ kilohertz interaction strengths [51,66] typical of most molecules. Nevertheless, several approaches have been developed to match the polarizabilities of two specific states within a molecule. These include judicious choice of the intensity and polarization of the trapping light [67–69] and the addition of applied electric fields to simplify the couplings within the molecule [65,66,70].

Inspired by the magic-wavelength traps used in atomic clocks [71,72], it is natural to investigate magic-wavelength trapping for molecules. Intuitively, magic trapping independent of the molecular rotational state can be realized under the condition of  $\alpha^{(2)} = 0$ . To search for this condition, one needs to tune the trapping laser wavelength into a regime where there is significant interplay between several rovibrational poles in  $\alpha_{\parallel}$  and  $\alpha_{\perp}$ . Indeed, following this approach, very recent work has demonstrated state-insensitive trapping for two vibrational [73] or rotational [74] levels. These magic-frequency traps show reduced sensitivity to experimental parameters, enabling longer coherence times to be achieved. However, numerous proposed applications make greater use of the rich internal structure of molecules by simultaneously addressing *more than two* rotational levels. Examples include coupling three rotational levels with microwave fields to realize highly tunable models in quantum magnetism [57] and mapping many rotational levels onto a synthetic dimension [75]. It is therefore pertinent to ask whether the concept of a magic frequency trap can be extended to multiple rotational levels simultaneously.

In this work, we investigate magic-wavelength trapping of ultracold alkali molecules in the vicinity of weak optical transitions from the vibrational ground state of the  $X^1\Sigma^+$  potential to low-lying rovibrational states of the  $b^3\Pi_0$  potential, focusing our discussion on the  $^{87}\text{Rb}^{133}\text{Cs}$  molecule. We show that a magic trapping frequency window for multiple rotational states of the  $X^1\Sigma^+$  potential exists between two nearest-neighbor vibrational poles of the  $b^3\Pi_0$  potential, far away from any rotational poles. Within this window, the laser trapping is “near magic” for multiple rotational states simultaneously and is exactly magic for pairs of neighboring rotational states at specific laser frequencies. Moreover, the “near magic” frequency window can be tuned to a true magic frequency for the lowest three rotational states by applying an experimentally accessible DC electric field. This true triple magic condition is expected to be useful for future studies of synthetic spin-1 systems using ultracold molecules. The existence of such a magic frequency window relies on a set of strict criteria which we derive analytically. We show that these criteria can be satisfied near the narrow  $X^1\Sigma^+ \rightarrow b^3\Pi_0$  transitions for heavy molecules, including  $^{87}\text{Rb}^{133}\text{Cs}$  and  $^{23}\text{Na}^{87}\text{Rb}$ . We also derive an analytic expression for the position of the frequency window in terms of a set of experimentally measurable parameters, such as transition widths and transition wavelengths. This will provide a straightforward, self-consistent approach to search for the magic trapping frequency window in future experiments.

This paper is organized as follows. Section II presents the general theoretical framework describing the molecular rotational states in the lowest vibrational state of the ground electronic potential in the presence of applied magnetic, electric, and optical fields. In Sec. III, we discuss the hyperfine structure of the  $^{87}\text{Rb}^{133}\text{Cs}$  molecule in the presence of applied magnetic and electric fields with a view to identifying the best target states in each rotational level for magic trapping. In Sec. IV, we consider the AC Stark shift and dynamic polarizability of  $^{87}\text{Rb}^{133}\text{Cs}$  molecules in the vicinity of the weakly allowed  $X^1\Sigma^+ \rightarrow b^3\Pi_0$  transitions. In Sec. V, we identify magic trapping frequencies by searching for crossings among

the frequency-dependent dynamic polarizability curves of different rotational states. We present a simple analytic treatment that shows excellent agreement with our numerical results, both near resonance and in the magic frequency window between two vibrational poles. Imaginary polarizabilities for rotational states in the magic frequency window are also calculated. In Sec. VI, we discuss the wider significance of our work, before concluding in Sec. VII.

## II. THEORETICAL FRAMEWORK

We focus on the molecular rotational states  $\vec{J}$  associated with the  $v = 0$  vibrational state of the ground electronic state of RbCs. The effective Hamiltonian that describes the system in the presence of a static magnetic field  $\vec{B}$ , a static electric field  $\vec{E}$ , and an optical laser field of intensity  $I$  [52,65,76] is given by

$$H = H_{\text{rot}} + H_Z + H_{\text{hf}} + H_{\text{DC}} + H_{\text{AC}}, \quad (2)$$

where the rotational Hamiltonian is

$$H_{\text{rot}} = B_v \vec{J}^2, \quad (3)$$

the Zeeman Hamiltonian is

$$H_Z = -g_r \mu_N \vec{J} \cdot \vec{B} - \sum_{k=1}^2 g_k \mu_N \vec{I}_k \cdot \vec{B} (1 - \sigma_k), \quad (4)$$

the nuclear quadrupole interaction is

$$H_{\text{hf}} = \sum_{k=1}^2 \frac{(eqQ)_k}{I_k(I_k - 1)} C_2(\alpha, \beta) T_2(\vec{I}_k, \vec{I}_k), \quad (5)$$

and the DC Stark shift is

$$H_{\text{DC}} = -\vec{d} \cdot \vec{E}. \quad (6)$$

In Eqs. (3)–(6)  $\vec{J}$ ,  $\vec{I}_k$ , and  $\vec{d}$  denote the molecule orbital angular momentum operator, the nuclear spin operators for the  $k$ th atom, and the permanent molecular electric dipole moment operator, respectively. The nuclear quadrupole interaction  $H_{\text{hf}}$  couples the nuclear spin to rotational states and depends on the quadrupole coupling constants  $(eqQ)_k$  for Rb and Cs obtained from Ref. [52]. The operator  $T_2(\vec{I}_k, \vec{I}_k)$  is a rank-2 tensor and  $C_2(\alpha, \beta) = \sqrt{4\pi/5} Y_{20}(\alpha, \beta)$  is the modified spherical harmonic function, where the angles  $\alpha, \beta$  describe the orientation of the diatomic molecule in the space-fixed coordinate frame. In these equations  $B_v$  is the rotational constant,  $\mu_N$  is the nuclear magneton, and  $g_r$  is the molecule rotational  $g$  factor. Moreover,  $g_k$  and  $\sigma_k$  with  $k = 1, 2$  are nuclear-spin  $g$  factors and isotropic molecular nuclear shielding factors, respectively.

Here, the direction of the external magnetic field is our quantization axis along which we define projection quantum numbers of angular momenta. The matrix elements of the Hamiltonian are determined in a low-energy set of basis functions  $|J, M; m_1, m_2\rangle$ , where  $J$  and  $M$  are the orbital angular momentum and its associated projection, respectively. Quantum numbers  $m_k$  are nuclear spin projections of the  $k$ th atom.

The AC Stark Hamiltonian  $H_{\text{AC}}$  in Eq. (2) is constructed up to second order in the electric field strength of the driving laser in the regime where the AC Stark shift is much smaller

than the rotational constant. In this regime, the AC Stark Hamiltonian  $H_{AC}$  is

$$H_{AC} = -\frac{I}{\epsilon_0 c} \sum_{\substack{J, M, M', \\ m_1, m_2}} |J, M'; m_1, m_2\rangle \langle J, M; m_1, m_2| \times \sum_f \frac{\langle J, M' | \vec{d}_{tr} \cdot \vec{\epsilon}^* | f \rangle \langle f | \vec{d}_{tr} \cdot \vec{\epsilon} | J, M \rangle}{E_f - (E_J + \hbar\omega)}, \quad (7)$$

where energies  $E_J$  are the eigenvalues of  $H_{rot}$ , and  $\vec{d}_{tr}$ ,  $\vec{\epsilon}$ , and  $\omega$  are the molecular transition electric dipole moment operator, the laser polarization, and the laser angular frequency, respectively. The summations over  $J$ ,  $M$ ,  $M'$ , and  $m_k$  only contain basis functions in the low-energy space. The summation  $f$  in Eq. (7) is over all rovibrational states and continua of excited electronic states with energies  $E_f$  excluding their Zeeman, hyperfine, and DC Stark shifts. We have included previously studied [63,70] excited electronic states that dissociate to limits where only one of Rb or Cs is excited to its energetically lowest excited  $nP$  state. In this work, we are interested in the regime where the AC Stark shift is much smaller than the rotational constant. Thus, in writing Eq. (7), couplings between the states with different orbital angular momenta  $J$  are neglected. Finally,  $\epsilon_0$ ,  $c$ , and  $\hbar$  are the vacuum permittivity, the speed of light in vacuum, and the reduced Planck constant, respectively.

We diagonalize Eq. (2) in the basis  $|J, M; m_1, m_2\rangle$  including  $J \leq 20$  to find eigenenergies  $E_i$  and corresponding eigenstates  $|i\rangle$  of the molecular system. The dynamic polarizability of an eigenstate is  $-\partial E_i / \partial I$ . By mapping out the intensity dependence of the eigenenergies of the effective low-energy Hamiltonian, we obtain the dynamic polarizabilities for various rotational states. The electric field, magnetic field, and laser frequency serve as our tuning parameters which can be manipulated, as shown in the following discussions, to realize various magic trapping conditions. Although in this work we focus our discussion on the  $^{87}\text{Rb}^{133}\text{Cs}$  molecule, the extension to other diatomic alkali molecules is implied.

### III. ZEEMAN SPLITTINGS AND DC STARK SHIFTS IN RBCS MOLECULES

The nuclear spins of  $^{87}\text{Rb}$  and  $^{133}\text{Cs}$  atoms are  $I_1 = 3/2$  and  $I_2 = 7/2$ , respectively. Because of the multiple combinations of the atomic nuclear spin projections and the molecular orbital angular momentum projections, there exist  $(2J+1)(2I_1+1)(2I_2+1)$  energy levels that are associated with the rotational state with orbital angular momentum  $J$ . In the presence of the magnetic field, the static electric field, and the hyperfine interactions, these ‘‘near’’ degenerate energy levels split. Before we discuss the magic trapping conditions, it is necessary to select the best target states to be trapped among these levels for each rotational state.

Figures 1(a), 1(c), and 1(e) show the hyperfine energy levels of the rotational  $J = 0, 1$ , and  $2$  manifolds of the  $v = 0$   $X$  state, respectively. The hyperfine degeneracy of a  $J$  state is lifted by an external magnetic field  $B$ . In this regime, the total angular momentum  $\vec{F}^2 = (\vec{J} + \vec{I}_1 + \vec{I}_2)^2$  and the total projection  $M_F = M + m_1 + m_2$  are approximately good quantum

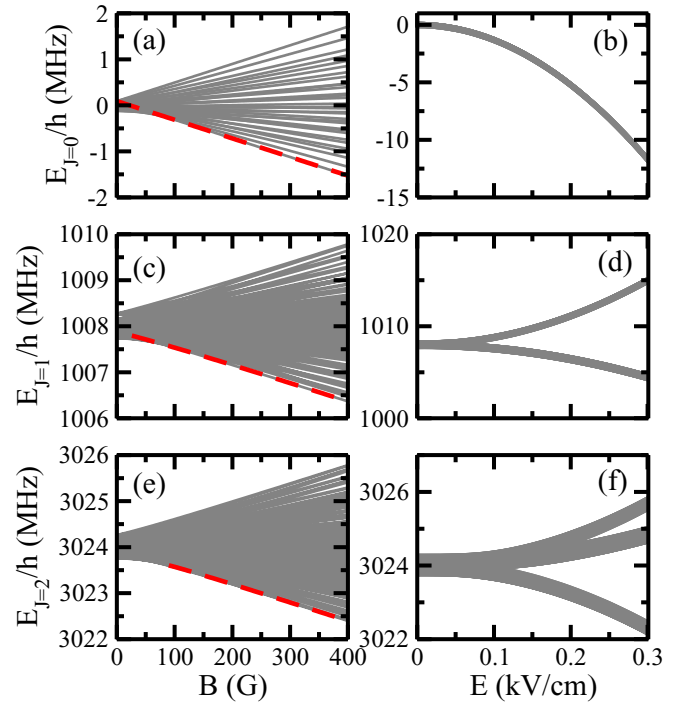


FIG. 1. The hyperfine energy levels for the  $J = 0, 1$ , and  $2$  manifolds as functions of the magnetic field strength  $B$  [(a), (c), and (e), respectively] and the static electric field strength  $E$  applied parallel to a magnetic field of  $B = 181$  G [(b), (d), and (f), respectively]. The red dashed lines in (a), (c), and (e) mark the target trapping state (see text). Panel (b) consists of a band with 32 energy levels. Panel (d) consists of two bands: the upper one contains 32 energy levels with  $M = 0$  and the lower one 64 energy levels with  $M = \pm 1$ . Panel (f) consists of three bands: the upper one contains 32 energy levels with  $M = 0$ , the middle one 64 energy levels with  $M = \pm 1$ , and the lower one 64 energy levels with  $M = \pm 2$ .

numbers, which means that the eigenstates consist of a strong admixture of states with different nuclear spin projections. The level repulsion is strong, leading to quadratic Zeeman shifts dominating over linear Zeeman shifts for  $B < 50$  G. With increasing magnetic field strength, the linear Zeeman shift dominates. Due to the differences in the various  $g$  factors,  $g_r = 0.0062$ ,  $g_1 = 1.836(3)$ , and  $g_2 = 0.738(1)$  in Eq. (4) for  $^{87}\text{Rb}^{133}\text{Cs}$  [52,77], the projections  $M$ ,  $m_1$ , and  $m_2$  are all approximately good quantum numbers in the high-field regime.

The red dashed lines in Figs. 1(a), 1(c), and 1(e) indicate the energetically lowest levels of these manifolds, which are selected as our target trapping states. For  $B > 150$  G, the admixture of the other components into the target trapping states is less than 20% for  $J = 0, 1$ , and  $2$ . In this paper, we focus on a magnetic field strength of  $B = 181$  G applied in the experiment [37]. In the additional presence of a static electric field, as shown in Figs. 1(b), 1(d), and 1(f), these target states are more purified and decoupled from  $|M| > 0$  states, thereby enhancing their tunability and improving magic trapping conditions. Thus, the static electric field separates the  $J = 0$ ,  $J = 1$ , and  $J = 2$   $M = 0$  levels from  $|M| > 0$  levels of the same manifolds. For  $B = 181$  G, a static electric field of strength  $E = 0.1$  kV/cm already makes the admixture of the states with finite  $M$  into the state with  $M = 0$  below 1%.

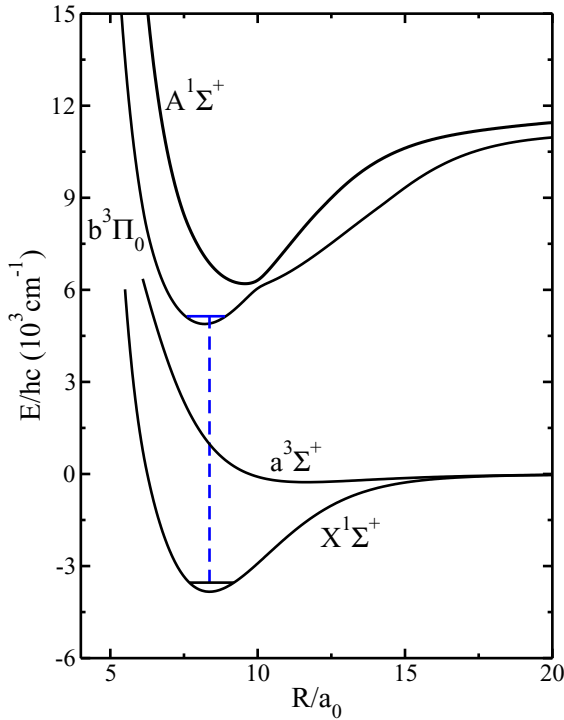


FIG. 2. Ground and relevant excited adiabatic relativistic  $\Omega = 0^+$  potentials of the  $^{87}\text{Rb}^{133}\text{Cs}$  molecule as a function of internuclear separation  $R$ . The energetically lowest potential is identified by the nonrelativistic label  $X^1\Sigma^+$ . The two excited adiabatic potentials have a narrow avoided crossing at  $R_c \approx 10a_0$ . For  $R < R_c$  the electronic wavefunction of the second adiabat is well described by the nonrelativistic  $b^3\Pi_0$  symmetry. For  $R > R_c$  this state is well described by the  $A^1\Sigma^+$  symmetry. The vertical lines indicate transitions from the  $J = 0$  trapping state in the  $X^1\Sigma^+$  state to the lowest  $J' = 1$  rovibrational states of the coupled  $A^1\Sigma^+ - b^3\Pi_0$  complex. The transition wavelength is 1146.287 nm.

#### IV. AC STARK SHIFTS NEAR THE NARROW $X^1\Sigma^+ \rightarrow b^3\Pi_0$ TRANSITIONS

To study the AC Stark shift of the  $^{87}\text{Rb}^{133}\text{Cs}$  molecule, we consider the application of a driving laser field with the angular frequency  $\omega$  to induce coupling between the target trapping states and electronically excited states. Figure 2 shows the selected relativistic adiabatic  $\Omega = 0^+$  potential curves of the  $^{87}\text{Rb}^{133}\text{Cs}$  molecule, where  $\Omega$  is the total projection quantum number of the electronic angular momentum and nuclear spins along the diatomic molecule axis. The  $b^3\Pi_0$  potential and the  $A^1\Sigma^+$  potential are coupled by the spin-orbit coupling terms which lead to an avoided crossing near  $R_c = 10a_0$ . Here, the potentials and the spin-orbit coupling functions are generated based on the data in Refs. [64,78–80]. Due to the spin-orbit coupling, the few lowest bound states lying near the bottom of the  $b^3\Pi_0$  potential have some admixture of the  $A^1\Sigma^+$  component which enables the electric dipole coupling from these states to the states of the ground electronic potential  $X^1\Sigma^+$ . These transitions are much narrower than the transitions to the states with dominant occupation in the  $A^1\Sigma^+$  potential. In this work, we are particularly interested in the AC Stark shift and the dynamic polarizabilities near these narrow transitions,

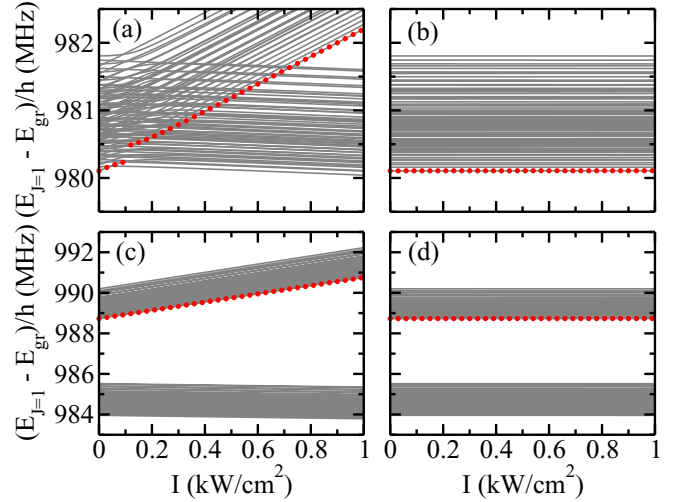


FIG. 3. Microwave transition frequencies from the  $|J = 0, M = 0; m_1 = 3/2, m_2 = 7/2\rangle$  ground state to the  $J = 1$  manifold as a function of the laser intensity for a laser frequency near the resonance transition to the  $v' = 0$  vibrational state of the  $b^3\Pi_0$  potential. A magnetic field of strength  $B = 181$  G is applied in the  $z$  direction. Panels (a) and (c) correspond to a detuning of  $\Delta_{v'=0} = 2\pi \times 3$  GHz. Panels (b) and (d) correspond to a detuning of  $\Delta_{v'=0} = 2\pi \times 200$  GHz. Panels (a) and (b) correspond to vanishing static electric field. Panels (c) and (d) correspond to a static electric field of  $E = 0.2$  kV/cm applied in the  $z$  direction. The red circles in all panels mark the energy level of the target trapping state.

indicated by the blue dashed line in Fig. 2. We denote  $\omega_{v'}$  the resonance transition frequency from the  $(v = 0, J = 0)$  state of the  $X^1\Sigma^+$  potential to the  $(v', J = 1)$  state of the  $b^3\Pi_0$  potential. For  $v' = 0$ , the resonance frequency reads  $\omega_0 = 2\pi \times 261.533$  THz which corresponds to a wavelength of 1146.287 nm. When the driving laser frequency  $\omega$  is close to the resonance frequency  $\omega_{v'}$ , we reference  $\omega$  to  $\omega_{v'}$  through the detuning  $\Delta_{v'} = \omega - \omega_{v'}$ .

Figure 3 shows the impact of the static electric field on the AC Stark shifts of the microwave transition frequencies from the  $|J = 0, M = 0; m_1 = 3/2, m_2 = 7/2\rangle$  ground state to the  $J = 1$  rotational energy manifold in the small and large detuning regimes. The driving laser is linearly polarized with a polarization parallel to the magnetic field. The red circles correspond to the target trapping state as discussed in Sec. III. For the case with the detuning of  $\Delta_{v'=0} = 2\pi \times 3$  GHz and vanishing static electric fields [Fig. 3(a)], the AC Stark shifts can be characterized into two bands: one going up with increasing laser intensity while the other stays almost independent of the laser intensity. The former corresponds to states with  $M = 0$  and the latter to states with  $M = \pm 1$ . As shown by the red circles in Fig. 3(a), the energy level of the target trapping state in the  $J = 1$  manifold crosses those of the other levels with increasing laser intensity. These crossings lead to strong level interactions [see the gap in the red circles near  $I = 0.1$  kW/cm<sup>2</sup> in Fig. 3(a)] and hence to large hyperpolarizabilities, which makes the system unstable with respect to fluctuations of the trapping laser intensity.

The level-crossing behavior in the AC Stark shift can be avoided by separating the  $M = 0$  band and the  $M = \pm 1$  band

using a static electric field as discussed in Sec. III. Figure 3(c) shows the AC Stark shifts in the presence of a static electric field of  $E = 0.2$  kV/cm. Compared to Fig. 3(a), the  $M = 0$  band lies roughly 5 MHz above the  $M = \pm 1$  band for  $I = 0$ . With increasing laser intensity, the energy gap between the  $M = 0$  band and the  $M = \pm 1$  band keeps increasing. The energy of the target trapping state does not cross any of the  $M = \pm 1$  states anymore.

The level crossings seen in Fig. 3(a) result from the fact that the AC Stark shift of the target trapping state is larger than the energy splitting between the nearest-neighbor hyperfine levels. With larger laser detuning, the differential AC Stark shift is greatly reduced. For example, for a detuning of  $\Delta_{v'=0} = 2\pi \times 200$  GHz as shown in Fig. 3(b), the level crossings between the target trapping state and the other states in the  $J = 1$  manifold disappear for the laser intensity regime shown here. As shown in Fig. 3(d), a static electric field separates the  $M = 0$  band from the  $M = \pm 1$  band. This further decreases  $M$ -state admixtures and improves coherence.

In the following discussion of dynamic polarizabilities, we describe the detuning as near resonance when  $\Delta_{v'} < 2\pi \times 10$  GHz and as medium detuned otherwise. According to the above discussion, the static electric field is always turned on for the near-resonance cases and not mandatory for the far-detuned cases. This setup makes our results independent of the laser intensity in a broad intensity regime for both cases.

## V. MAGIC CONDITIONS FOR MULTIPLE ROTATIONAL STATES

We may identify magic trapping frequencies by searching for crossings among the frequency-dependent dynamic polarizability curves of different rotational states. We start the discussion with the dynamic polarizabilities  $\alpha_J$  near the resonance from which we extract the parallel and perpendicular background polarizabilities  $\alpha_{\text{bg},\parallel}$  and  $\alpha_{\text{bg},\perp}$  and the transition width  $\Gamma_{0,v'}$ . Given the values of  $\alpha_{\text{bg},\parallel}$ ,  $\alpha_{\text{bg},\perp}$ , and  $\Gamma_{0,v'}$ , it is proved analytically and verified by our numerical calculations that there exists a “near” magic frequency window for multiple rotational states in the medium-detuned regime between vibrational poles. By tuning the static electric field, a true triple magic frequency is found for the  $J = 0$ ,  $J = 1$ , and  $J = 2$  target trapping states for the  $^{87}\text{Rb}^{133}\text{Cs}$  molecule.

### A. Near-resonance dynamic polarizabilities

In the near-resonance regime, we fix the strength of the static electric field to be  $E = 0.2$  kV/cm. The angle between the laser polarization and the magnetic field is denoted  $\theta$ . In this case, the dynamic polarizabilities  $\alpha_{J=0}$  of the  $J = 0$ ,  $M = 0$  target trapping state and  $\alpha_{J=1}$  of the  $J = 1$ ,  $M = 0$  target trapping state can be approximated using Ref. [67] by

$$\alpha_{J=0} = -\frac{3\pi c^2}{2\omega_{v'}^3} \frac{\Gamma_{0,v'}}{3\Delta_{v'}} + \frac{1}{3}\alpha_{\text{bg},\parallel} + \frac{2}{3}\alpha_{\text{bg},\perp}, \quad (8)$$

and

$$\alpha_{J=1} = -\frac{3\pi c^2}{2\omega_{v'}^3} \left[ \frac{\cos^2(\theta)}{3} \frac{\Gamma_{0,v'}}{\Delta_{v'} + 2B_v + 2B_{v'}} \right]$$

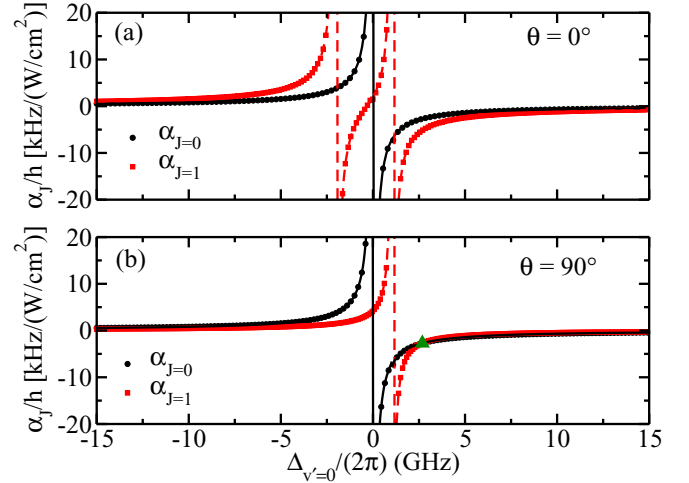


FIG. 4. The dynamic polarizabilities near the resonance transition to the  $v = 0$  vibrational state of the  $b^3\Pi_0$  potential. A magnetic field of strength  $B = 181$  G and a static electric field of strength  $E = 0.2$  kV/cm are applied in the  $z$  direction. The driving laser polarization is (a) parallel and (b) perpendicular to the external static fields. The black circles and red squares correspond to the numerical results of the dynamic polarizabilities of the  $J = 0$  and  $J = 1$  target trapping state. The black solid lines and the red solid lines correspond to the analytical results generated using Eqs. (8) and (9). The green triangle in (b) marks the crossing between the black circles and red squares.

$$+ \frac{3 + \cos^2(\theta)}{15} \frac{\Gamma_{0,v'}}{\Delta_{v'} + 2B_v - 4B_{v'}} \left. \right] + \frac{2\cos^2(\theta) + 1}{5}\alpha_{\text{bg},\parallel} + \frac{4 - 2\cos^2(\theta)}{5}\alpha_{\text{bg},\perp}, \quad (9)$$

respectively. Here, the parameters  $B_v$  and  $B_{v'}$  correspond to the rotational constants for the  $v = 0$  vibrational state of the  $X^1\Sigma^+$  potential and the  $v' = 0$  vibrational state of the  $b^3\Pi_0$  potential. The transition width  $\Gamma_{0,v'}$  can be calculated via

$$\Gamma_{0,v'} = \frac{\omega_{v'}^3}{3\pi\epsilon_0\hbar c^3} |\mu_{0,v'}|^2, \quad (10)$$

where the  $\mu_{0,v'}$  is the transition dipole moment between the  $v = 0$  vibrational state of the  $X^1\Sigma^+$  potential and the  $v'$  vibrational state of the  $b^3\Pi_0$  potential. The parallel and perpendicular background polarizabilities  $\alpha_{\text{bg},\parallel}$  and  $\alpha_{\text{bg},\perp}$  contain the contributions from all the far-detuned rovibronic states with  $\Omega = 0$  and  $\Omega = 1$ , respectively [63–65]. For  $^{87}\text{Rb}^{133}\text{Cs}$ , we find  $B_v = 2\pi \times 0.490$  GHz,  $B_{v'} = 2\pi \times 0.510$  GHz,  $\Gamma_{0,v'=0} = 2\pi \times 15.5$  kHz,  $\alpha_{\text{bg},\parallel} = h \times 0.127$  kHz/(W/cm<sup>2</sup>), and  $\alpha_{\text{bg},\perp} = h \times 0.0340$  kHz/(W/cm<sup>2</sup>). Experimentally, these values can be extracted by fitting the measured dynamic polarizability curves near the poles.

Figure 4 shows the dynamic polarizabilities for laser polarizations parallel and perpendicular to the magnetic field direction in the near-resonance regime. The symbols correspond to the numerical results and the lines show the analytical results generated using Eqs. (8) and (9). The agreement in both cases is excellent. As can be seen, there is no crossing between the  $\alpha_{J=0}$  curve and the  $\alpha_{J=1}$  curve in

the near-resonance regime for  $\theta = 0^\circ$ . According to Eq. (9), the dynamic polarizability  $\alpha_{J=1}$  can be tuned by varying the polarization direction of the driving laser. For example, for  $\theta = 90^\circ$ , the term in the first row of Eq. (9) inside the square bracket vanishes and the pole structure at  $\Delta_{v'=0} = -2\pi \times 2.00$  GHz is missing, as shown by the red squares in Fig. 4(b). In addition, the pole at  $\Delta_{v'=0} = 2\pi \times 1.06$  GHz is slightly narrower compared to the  $\theta = 0^\circ$  case. In this case, the  $\alpha_{J=1}$  curve crosses the  $\alpha_{J=0}$  curve at the magic detuning of  $2\pi \times 2.68$  GHz, as shown by the green triangle in Fig. 4(b). The value of the polarizability at the magic detuning is  $-h \times 2.71$  kHz/(W/cm<sup>2</sup>). The negative polarizability indicates that the molecules can be trapped at the nodal point of an optical lattice where the laser intensity is the local minimum. This trapping condition is beneficial for also minimizing heating and loss from incoherent photon scattering.

### B. Multiple magic frequency window

For arbitrary  $J$ , we derive the general formula for the dynamic polarizability near the resonance transition to one of the states of the  $b^3\Pi_0$  potential,

$$\alpha_J = -\frac{3\pi c^2}{2\omega_{v'}^3} \left[ A_J(\theta) \frac{\Gamma_{0,v'}}{\Delta_{v'} + L_J} + B_J(\theta) \frac{\Gamma_{0,v'}}{\Delta_{v'} + R_J} \right] + [A_J(\theta) + B_J(\theta)]\alpha_{\text{bg},\parallel} + [1 - A_J(\theta) - B_J(\theta)]\alpha_{\text{bg},\perp}, \quad (11)$$

where the pole positions  $L_J$  of the left branch and  $R_J$  of the right branch read

$$L_J = J(J+1)B_v - [J(J-1) - 2]B_{v'} \quad (12)$$

and

$$R_J = J(J+1)B_v - [(J+1)(J+2) - 2]B_{v'}, \quad (13)$$

respectively. The angular factors  $A_J(\theta)$  and  $B_J(\theta)$  in Eq. (11) are

$$A_J(\theta) = \begin{cases} \frac{(J+1)(J-1)}{2(2J+1)(2J-1)} \\ + \frac{J^2+1}{2(2J+1)(2J-1)} \cos^2(\theta), & J > 0 \\ 0, & J = 0, \end{cases} \quad (14)$$

and

$$B_J(\theta) = \frac{(J+2)(J+1)}{2(2J+3)(2J+1)} + \frac{J(J+1)}{2(2J+3)(2J+1)} \cos^2(\theta). \quad (15)$$

By Taylor-expanding the right-hand side of Eq. (11) with respect to  $L_J$  and  $R_J$ , we obtain

$$\alpha_J = [A_J(\theta) + B_J(\theta)] \left( -\frac{3\pi c^2}{2\omega_{v'}^3} \frac{\Gamma_{0,v'}}{\Delta_{v'}} + \alpha_{\text{bg},\parallel} - \alpha_{\text{bg},\perp} \right) + \alpha_{\text{bg},\perp} + T_J(\Delta_{v'}, \theta), \quad (16)$$

where the remaining term  $T_J(\Delta_{v'}, \theta)$  reads

$$T_J(\Delta_{v'}, \theta) = \frac{3\pi c^2}{2\omega_{v'}^3} \frac{\Gamma_{0,v'}}{\Delta_{v'}^2} [A_J(\theta)L_J + B_J(\theta)R_J] + O\left(\frac{\Gamma_{0,v'}L_J^2}{\Delta_{v'}^3}\right) + O\left(\frac{\Gamma_{0,v'}R_J^2}{\Delta_{v'}^3}\right). \quad (17)$$

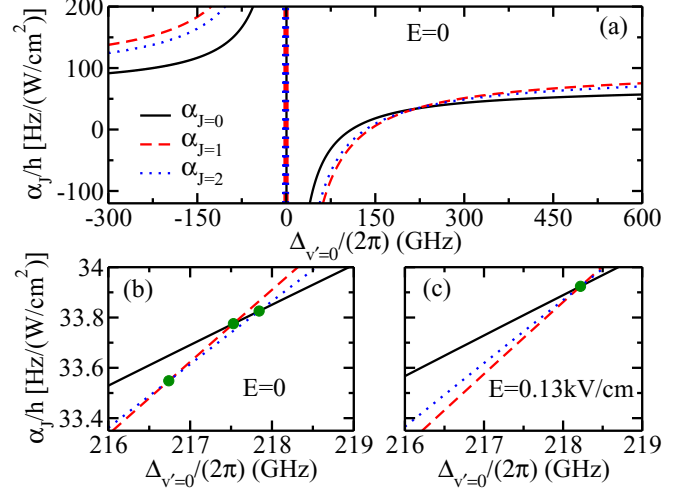


FIG. 5. The triple magic conditions for  $J = 0, 1$ , and  $2$  rotational states near the resonance transition to the  $v = 0$  state of the  $b^3\Pi_0$  potential. A magnetic field  $B = 181$  G is applied in the  $z$  direction. The laser polarization is parallel to the magnetic field. The circles mark the crossings between different curves in (b) and (c). The static electric field is vanishing in (a) and (b). A finite static electric field of  $E = 0.13$  kV/cm is applied along the  $z$  direction in (c). A near triple magic condition exists in (b) and a true triple magic condition exists in (c).

Based on Eq. (16), we can always find a detuning  $\Delta_{v',\text{cr}}$  such that

$$\alpha_J = \alpha_{\text{bg},\perp} + T_J(\Delta_{v',\text{cr}}, \theta), \quad (18)$$

where

$$\Delta_{v',\text{cr}} = \frac{3\pi c^2}{2\omega_{v'}^3} \frac{\Gamma_{0,v'}}{\alpha_{\text{bg},\parallel} - \alpha_{\text{bg},\perp}}. \quad (19)$$

For the transitions with  $\Delta_{v',\text{cr}}$  lying in the medium-detuned regime, i.e.,  $|\Delta_{v',\text{cr}}| \gg |L_J|$ ,  $|\Delta_{v',\text{cr}}| \gg |R_J|$ , and  $|\Delta_{v',\text{cr}}| \gg \Gamma_{0,v'}$ , the remaining term  $T_J(\Delta_{v',\text{cr}}, \theta)$  can be neglected. In this case, both the  $\theta$  dependence and the  $J$  dependence of  $\alpha_J$  in Eq. (18) disappear, indicating that the frequency-dependent dynamic polarizabilities of all rotational states pass through the same fixed point; the trap is magic for all rotational states at this laser detuning. The multiple magic frequency is approximately given by Eq. (19) and the value of the dynamic polarizability is approximately equal to the background perpendicular dynamic polarizability  $\alpha_{\text{bg},\perp}$ .

Figure 5(a) shows the triple crossing magic frequency for  $\alpha_J$  with  $J = 0, 1$ , and  $2$  near the resonance transition to the  $v' = 0$  vibrational states of the  $b^3\Pi_0$  potential. The three curves cross each other in the detuning window of  $2\pi \times 216$  to  $2\pi \times 219$  GHz, as highlighted in Fig. 5(b). Evaluating Eq. (19) using the values of the transition width and the background polarizabilities obtained in Sec. V A, the predicted magic frequency corresponds to a detuning of  $2\pi \times 240$  GHz. The difference comes from the higher-order corrections in the remaining term  $T_J(\Delta_{v'}, \theta)$ . The range of the  $\alpha_J$  values in Fig. 5(b) is consistent with the value of  $\alpha_{\text{bg},\perp}$  as calculated in Sec. V A. Even though the three curves do not intersect each other at the same frequency, their values are very close in the

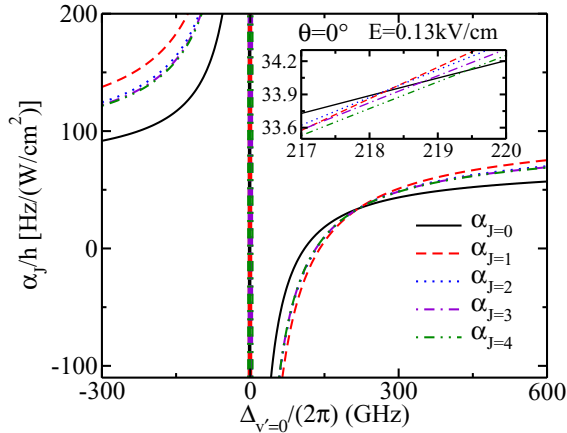


FIG. 6. The dynamic polarizabilities near the resonance transition to the  $v = 0$  vibrational state of the  $b^3\Pi_0$  potential for multiple rotational states up to  $J = 4$ . A magnetic field of  $B = 181$  G and a static electric field of  $E = 0.13$  kV/cm are applied in the  $z$  direction. The laser polarization is parallel to the  $z$  axis. The insets show the zoom-in of the “near magic” frequency window in which the polarizabilities of many rotational states are either crossing or close to each other.

frequency window shown in Fig. 5(b). The percent difference  $|\alpha_J - \alpha_{J'}|/|\alpha_{J'}|$  for any pair of  $J$  and  $J'$  in Fig. 5(b) is less than 0.6% within the detuning range of  $2\pi \times 3$  GHz, which makes the magic trapping condition robust to uncertainty in the trapping laser frequency. This near triple magic frequency window can be tuned to a true triple magic frequency by adding a weak static electric field. Figure 5(c) shows that the three curves cross at  $\Delta_{v'=0} = 2\pi \times 218.22$  GHz for  $E = 0.13$  kV/cm. The value of the polarizability at this detuning is  $\alpha_J = h \times 0.03392$  kHz/(W/cm<sup>2</sup>).

Our theory also predicts that the triple magic frequency window also holds for higher rotational states. Figure 6 shows the  $\alpha_J$  curves up to  $J = 4$  for the parallel driving case in the presence of the static electric field of strength  $E = 0.13$  kV/cm. It can be seen that all the values of  $\alpha_J$  are very close to  $\alpha_{\text{bg},\parallel}$  in the same magic frequency window as discussed before. A further zoom-in of the magic frequency window, shown in the inset of Fig. 6, indicates that  $\alpha_{J=3}$  and  $\alpha_{J=4}$  almost run parallel to  $\alpha_{J=2}$  and, consequently, do not pass through the triple magic frequency point for the  $\alpha_{J=0,1,2}$  curves. The higher rotational states make the contribution from the remaining term  $T_J(\Delta_{v',\text{cr}}, \theta)$  more important due to larger values of  $|L_J|$  and  $|R_J|$ . Thus, no crossings among the polarizability curves of higher  $J$  values are expected within the magic frequency window.

The similarity of the  $\alpha_J$  curves in the medium-detuned regime with increasing  $J$  values is explained by the asymptotic behavior of the angular factors  $A_J(\theta)$  and  $B_J(\theta)$  in Eqs. (14) and (15) in the large- $J$  limit. Expanding  $A_J(\theta)$  and  $B_J(\theta)$  in terms of  $1/J$ , we obtain

$$A_J(\theta) = \frac{1 + \cos^2(\theta)}{8} + O\left(\frac{1}{J^2}\right), \quad (20)$$

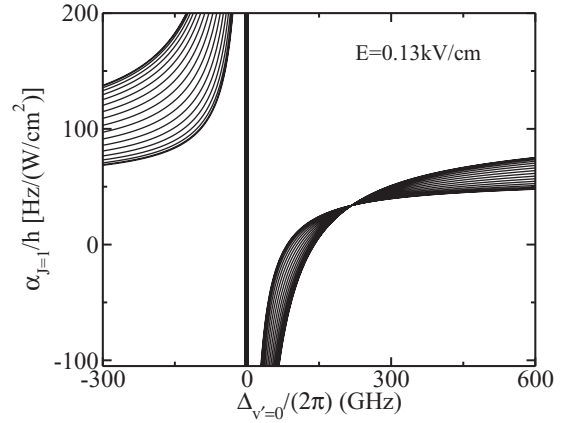


FIG. 7. The dynamic polarizabilities  $\alpha_{J=1}$  near the resonance transition to the  $v' = 0$  vibrational state of the  $b^3\Pi_0$  potential for various driving laser polarization directions. The angle  $\theta$  is scanned from  $0^\circ$  to  $90^\circ$  in  $5^\circ$  increments. A magnetic field of  $B = 181$  G and a static electric field of  $E = 0.13$  kV/cm are applied in the  $z$  direction.

and

$$B_J(\theta) = \frac{1 + \cos^2(\theta)}{8} + \frac{\sin^2(\theta)}{8J} + O\left(\frac{1}{J^2}\right). \quad (21)$$

With increasing  $J$ , the leading-order terms of both  $A_J(\theta)$  and  $B_J(\theta)$  are independent of the value of  $J$ ; hence the expression for  $\alpha_J$  in Eq. (16) becomes the same for all  $J$ , neglecting the remaining  $T_J(\Delta_{v'}, \theta)$  term. Thus, for large  $J$ , the various  $\alpha_J$  curves are close and almost parallel to each other in the medium-detuned regime. Combining the true triple magic condition for the lower  $J$  values and the similarity between  $\alpha_J$  for higher  $J$  values leads to a “near magic” trapping window for multiple rotational states that should be possible to realize experimentally.

The  $\theta$  dependence of  $\alpha_J$  within the multiple magic frequency window is also verified by our numerical results. Figure 7 shows the dynamic polarizability  $\alpha_{J=1}$  for angles between  $0^\circ$  and  $90^\circ$ . All the curves nearly cross the same point around the detuning of  $2\pi \times 218$  GHz.

Based on all the results and observations discussed above, we conclude that the existence of the multiple magic frequency window presents a frequency region of a few gigahertz within which the system is super robust with respect to the fluctuations of the trapping laser frequency and the polarization direction for arbitrary rotational states. Within this window long-rotational coherences should be possible on multiple rotational transitions in the  $^{87}\text{Rb}$   $^{133}\text{Cs}$  molecule.

### C. Criteria for the multiple magic frequency window

The existence of the multiple magic frequency window relies on the condition that the remaining  $T_J(\Delta_{v'}, \theta)$  term in Eq. (18) is much smaller than the  $\alpha_{\text{bg},\perp}$  and thus can be neglected. Taking the leading-order term of  $T_J(\Delta_{v'}, \theta)$  in Eq. (17), the condition  $|T_J(\Delta_{v',\text{cr}}, \theta)| \ll |\alpha_{\text{bg},\perp}|$  yields a lower bound on the transition width  $\Gamma_{0,v'}$  in terms of the background

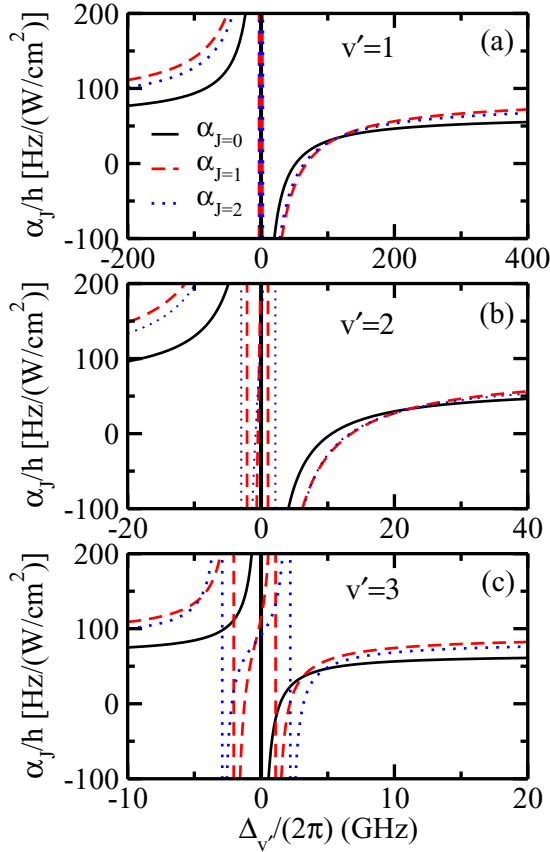


FIG. 8. The dynamic polarizabilities of the  $J = 0, 1,$  and  $2$  rotational states near the resonance transitions to the (a)  $v' = 1,$  (b)  $v' = 2,$  and (c)  $v' = 3$  vibrational states of the  $b^3\Pi_0$  potential. A magnetic field of  $B = 181$  G is applied in the  $z$  direction. No static electric field is applied. The black solid, red dashed, and blue dotted lines correspond to the dynamic polarizabilities of  $J = 0, 1,$  and  $2$  rotational states, respectively. A near triple magic condition exists in (a) and (b) but not in (c).

polarizabilities and rotational constants,

$$\Gamma_{0,v'} \gg \frac{2\omega_{v'}^3}{3\pi c^2} \frac{(\alpha_{\text{bg},\parallel} - \alpha_{\text{bg},\perp})^2}{|\alpha_{\text{bg},\perp}|} \sqrt{B_v^2 + B_{v'}^2}. \quad (22)$$

For  $^{87}\text{Rb}^{133}\text{Cs}$  molecules near the narrow transitions to the bottom of the  $b^3\Pi_0$  potential, the right-hand side of Eq. (22) is equal to  $2\pi \times 0.125$  kHz. As the transition linewidth  $\Gamma_{0,v'}$  decreases with increasing  $v'$ , this condition puts a constraint on the number of vibrational poles around which the multiple magic frequency window exists.

Figure 8 shows  $\alpha_J$  for  $J = 1, 2,$  and  $3$  near the  $v' = 1, 2,$  and  $3$  vibrational poles at the bottom of the  $b^3\Pi_0$  potential. With increasing  $v'$ , the transition is narrower and the triple crossing moves towards the pole of  $\alpha_J$ . The transition widths are  $\Gamma_{0,v'=1} = 2\pi \times 6.84$  kHz for the  $v' = 1$  pole and  $\Gamma_{0,v'=2} = 2\pi \times 1.44$  kHz for the  $v' = 2$  pole. Triple crossings can be seen around  $\Delta_{v'=1} = 2\pi \times 120$  GHz for the  $v' = 1$  vibrational pole [Fig. 8(a)] and around  $\Delta_{v'=2} = 2\pi \times 22$  GHz near the  $v' = 2$  vibrational pole [Fig. 8(b)]. For  $v' = 3$ , the transition width  $\Gamma_{0,v'=3}$  is  $2\pi \times 0.206$  kHz which is already

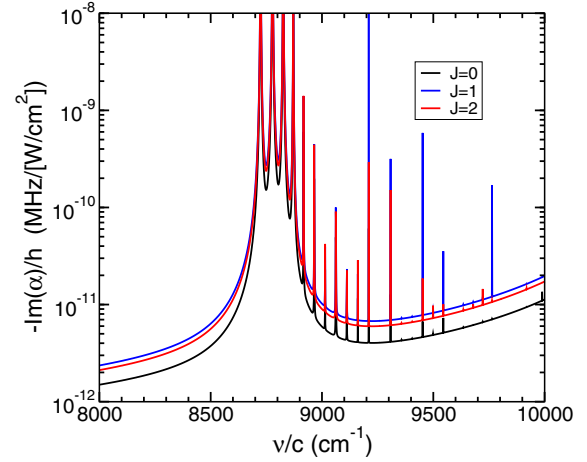


FIG. 9. The imaginary polarizabilities for the  $v = 0, J = 0, J = 1,$  and  $J = 2, M = 0$  states of the  $X^1\Sigma^+$  potential near the resonance transitions to the lower vibrational states of the  $b^3\Pi_0$  potential for  $\sigma_z$  polarization of the trapping light.

close to the lower bound. Thus, no triple crossings can be seen in Fig. 8(c).

#### D. Imaginary polarizability in the magic trapping window

Light-induced decoherence of rovibrational levels of a polar molecule is often characterized by the imaginary part of the polarizability [81], which accounts for losses due to spontaneous emission and other decay mechanisms of intermediate electronically excited states. Here, we evaluate the imaginary part of the complex molecular dynamic polarizability  $\alpha(\hbar\omega, \vec{\epsilon})$  as

$$\alpha(\hbar\omega, \vec{\epsilon}) = \frac{1}{\epsilon_0 c} \sum_f \frac{(E_f - ih\gamma_f/2 - E_i)}{(E_f - ih\gamma_f/2 - E_i)^2 - (\hbar\omega)^2} \times |(f|\vec{d}_{tr} \cdot \vec{\epsilon}|i)|^2, \quad (23)$$

assuming that each of these intermediate  $E_f$  states has a photon-induced coupling to the electronic ground-state linewidth  $\gamma_f$  equal to 6 MHz, the atomic linewidth of the Rb  $5p^2(P)$  state. This assumption is justified by previous calculations of the imaginary polarizability of rovibrational levels of ground-state KRb molecules [76] and a comparison of  $\alpha_{\text{imag}}$  with an experimentally measured value [81]. The sum over  $f$  in Eq. (23) is limited to transitions to relativistic electronic excited potentials that dissociate to either a singly excited Rb or a singly excited Cs atom.

Figure 9 shows the calculated imaginary part of the polarizability of the  $v = 0, J = 0, 1, 2 X^1\Sigma^+$  states as functions of laser frequency. By construction the imaginary part is negative. It is several orders of magnitude smaller than the real part. The resonances in the graph correspond to poles due to the lowest vibrational  $v'$  of the  $\Omega = 0$  relativistic component of the  $b^3\Pi_0$  potential. For a detuning of  $\Delta_{v'=0} = 2\pi \times 218$  GHz close to the triple magic frequency shown in Fig. 5, the value of the imaginary part of the polarizability is  $1.0 \times 10^{-9}$  kHz/(W/cm<sup>2</sup>). For comparison, the polarizability

at this detuning is  $\alpha_J = h \times 0.03392 \text{ kHz}/(\text{W}/\text{cm}^2)$ , as stated earlier.

## VI. DISCUSSION

Although all the results above are derived by considering transitions to the  $b^3\Pi_0$  potential, results similar to Eqs. (18) and (19) are found for  $\Omega = 1$  potentials with  $\alpha_{\text{bg},\perp}$  replaced by  $\alpha_{\text{bg},\parallel}$  and vice versa. These observations indicate that any rovibrational pole that is associated with a resonance transition to the state with quantum number  $\Omega$  can be used to cancel the contributions to the rank-2 dynamic polarizability tensor from all the other far-detuned states with the same quantum number  $\Omega$ . What remains is the contribution to the dynamic polarizability from the states with different  $\Omega$ . This cancellation happens at a frequency that is independent of the rotational quantum number  $J$  and the polarization direction of the laser.

Even though the derivation of the equations in Sec. VB is “universal,” i.e., independent of the molecule species, the existence of the magic frequency window does require certain conditions to be fulfilled. For example, Eq. (22) gives us a lower bound on the transition width. For heavier molecules, such as  $^{87}\text{Rb}^{133}\text{Cs}$ , this condition can be satisfied near the narrow transitions to the bottom of the  $b^3\Pi_0$  potential, since the spin-orbit coupling effect is stronger and the rotational constants,  $B_v$  and  $B_{v'}$ , are smaller. For  $^{23}\text{Na}^{87}\text{Rb}$ , we also find that the magic frequency window exists near the narrow transitions to the  $b^3\Pi_0$  potential. However, compared to  $^{87}\text{Rb}^{133}\text{Cs}$ , the window only exists near the  $v' = 0$  and  $v' = 1$  vibrational poles and is missing near the  $v' = 2$  pole.

Here, we emphasize that the condition on the lower bound of the transition width given by Eq. (22) is not the only criterion for the existence of the multiple magic frequency window. Equation (22) allows the multiple magic frequency window to also be found near broad transitions. However, in this case, the predicted magic frequency position in Eq. (19) cannot be larger than the energy spacing between two nearest-neighbor vibrational poles (i.e.,  $|\Delta_{v',cr}| \ll |\omega_{v'\pm 1} - \omega_{v'}|$ ). This condition puts an upper bound for the transition width,

$$\Gamma_{0,v'} \ll \frac{2\omega_{v'}^3}{3\pi c^2} |\alpha_{\text{bg},\parallel} - \alpha_{\text{bg},\perp}| \times |\omega_{v'\pm 1} - \omega_{v'}|, \quad (24)$$

where the “+/-” should be used for the positive or negative value of  $\alpha_{\text{bg},\parallel} - \alpha_{\text{bg},\perp}$ . This condition is very easily satisfied near the narrow transitions; however, it needs to be examined near the broad ones. This condition implies that we need to be in the “medium-detuned” regime to find the multiple magic frequency window.

We expect that our analytical formulas can be used for heteronuclear dimers other than RbCs and NaRb. To determine magic conditions for three and more rotational levels of the  $X$  potential of other alkali-metal molecules one needs to know the lifetime of the  $v = 0$   $b^3\Pi_0$  state, the rotational constant of the ground state, the vibrational spacings of the  $b^3\Pi_0$

potential, and the background dynamic polarizability at the transition frequency to the  $b^3\Pi_0$  potential. We only carefully studied RbCs and NaRb, as we could use potentials from the literature and computed all other characteristics ourselves.

Although the existence of the multiple magic frequency windows needs to be checked case by case, the results derived in this work will greatly benefit the search for them. In experiments, the background values of the polarizabilities and the transition widths can both be straightforwardly measured. According to Eq. (19), the magic detuning can then be predicted based entirely upon these measured values.

## VII. CONCLUSION

We have investigated magic-wavelength trapping of ultracold alkali molecules in the vicinity of weak optical transitions from the vibrational ground state of the  $X^1\Sigma^+$  potential to low-lying rovibrational states of the  $b^3\Pi_0$  potential, focusing our discussion on the  $^{87}\text{Rb}^{133}\text{Cs}$  molecule. We have shown that a magic trapping frequency window for multiple rotational states exists between two nearest-neighbor vibrational poles, far away from any rotational poles. Within this window, the laser trapping is “near magic” for multiple rotational states simultaneously and is exactly magic for pairs of neighboring rotational states at specific laser frequencies. Moreover, the “near magic” frequency window can be tuned to a true magic frequency for the lowest three rotational states by applying an experimentally accessible DC electric field. This true triple magic condition is expected to be useful for future studies of synthetic spin-1 systems using ultracold molecules.

We have derived a set of criteria that must be fulfilled to ensure the existence of such magic frequency windows and have also presented an analytic expression for the position of the frequency window in terms of a set of experimentally measurable parameters. These will provide a straightforward, self-consistent approach to search for the magic trapping frequency window in future experiments. We expect the realization of optical traps which are simultaneously magic for multiple rotational states will enable the implementation of highly tunable models in quantum magnetism [57] and the mapping of many rotational levels onto a synthetic dimension [75]. More broadly, our work is relevant in settings where there is a need to control the relative polarizabilities of different molecular rotational states, facilitating, for example, the study of Hopf insulators in dipolar systems [82].

## ACKNOWLEDGMENTS

S.L.C. acknowledges support from the UK Engineering and Physical Sciences Research Council (Grants No. EP/P01058X/1 and No. EP/P008275/1). Work at Temple University is supported by the Army Research Office Grant No. W911NF-17-1-0563, the U.S. Air Force Office of Scientific Research Grant No. FA9550-19-1-0272, and the National Science Foundation Grant No. PHY-1908634.

[1] L. D. Carr, D. DeMille, R. V. Krems, and J. Ye, *New J. Phys.* **11**, 055049 (2009).

[2] T. Zelevinsky, S. Kotochigova, and J. Ye, *Phys. Rev. Lett.* **100**, 043201 (2008).

- [3] E. J. Salumbides, G. D. Dickenson, T. I. Ivanov, and W. Ubachs, *Phys. Rev. Lett.* **107**, 043005 (2011).
- [4] E. J. Salumbides, J. C. J. Koelemeij, J. Komasa, K. Pachucki, K. S. E. Eikema, and W. Ubachs, *Phys. Rev. D* **87**, 112008 (2013).
- [5] M. R. Tarbutt, B. E. Sauer, J. J. Hudson, and E. A. Hinds, *New J. Phys.* **15**, 053034 (2013).
- [6] S. Schiller, D. Bakalov, and V. I. Korobov, *Phys. Rev. Lett.* **113**, 023004 (2014).
- [7] M. Borkowski, *Phys. Rev. Lett.* **120**, 083202 (2018).
- [8] M. Borkowski, A. A. Buchachenko, R. Ciuryło, P. S. Julienne, H. Yamada, Y. Kikuchi, Y. Takasu, and Y. Takahashi, *Sci. Rep.* **9**, 14807 (2019).
- [9] R. V. Krems, *Phys. Chem. Chem. Phys.* **10**, 4079 (2008).
- [10] M. T. Bell and T. P. Softley, *Mol. Phys.* **107**, 99 (2009).
- [11] S. Ospelkaus, K.-K. Ni, D. Wang, M. H. G. de Miranda, B. Neyenhuis, G. Quémener, P. S. Julienne, J. L. Bohn, D. S. Jin, and J. Ye, *Science* **327**, 853 (2010).
- [12] O. Dulieu, R. Krems, M. Weidemüller, and S. Willitsch, *Phys. Chem. Chem. Phys.* **13**, 18703 (2011).
- [13] N. Balakrishnan, *J. Chem. Phys.* **145**, 150901 (2016).
- [14] L. Santos, G. V. Shlyapnikov, P. Zoller, and M. Lewenstein, *Phys. Rev. Lett.* **85**, 1791 (2000).
- [15] A. Micheli, G. Pupillo, H. P. Büchler, and P. Zoller, *Phys. Rev. A* **76**, 043604 (2007).
- [16] L. Pollet, J. D. Picon, H. P. Büchler, and M. Troyer, *Phys. Rev. Lett.* **104**, 125302 (2010).
- [17] B. Capogrosso-Sansone, C. Trefzger, M. Lewenstein, P. Zoller, and G. Pupillo, *Phys. Rev. Lett.* **104**, 125301 (2010).
- [18] M. A. Baranov, M. Dalmonte, G. Pupillo, and P. Zoller, *Chem. Rev.* **112**, 5012 (2012).
- [19] W. Lechner and P. Zoller, *Phys. Rev. Lett.* **111**, 185306 (2013).
- [20] R. Barnett, D. Petrov, M. Lukin, and E. Demler, *Phys. Rev. Lett.* **96**, 190401 (2006).
- [21] A. Micheli, G. K. Brennen, and P. Zoller, *Nat. Phys.* **2**, 341 (2006).
- [22] H. P. Büchler, E. Demler, M. Lukin, A. Micheli, N. Prokof'ev, G. Pupillo, and P. Zoller, *Phys. Rev. Lett.* **98**, 060404 (2007).
- [23] A. Macià, D. Hufnagl, F. Mazzanti, J. Boronat, and R. E. Zillich, *Phys. Rev. Lett.* **109**, 235307 (2012).
- [24] S. R. Manmana, E. M. Stoudenmire, K. R. A. Hazzard, A. M. Rey, and A. V. Gorshkov, *Phys. Rev. B* **87**, 081106(R) (2013).
- [25] A. V. Gorshkov, K. R. A. Hazzard, and A. M. Rey, *Mol. Phys.* **111**, 1908 (2013).
- [26] D. DeMille, *Phys. Rev. Lett.* **88**, 067901 (2002).
- [27] S. F. Yelin, K. Kirby, and R. Côté, *Phys. Rev. A* **74**, 050301(R) (2006).
- [28] J. Zhu, S. Kais, Q. Wei, D. Herschbach, and B. Friedrich, *J. Chem. Phys.* **138**, 024104 (2013).
- [29] F. Herrera, Y. Cao, S. Kais, and K. B. Whaley, *New J. Phys.* **16**, 075001 (2014).
- [30] K.-K. Ni, T. Rosenband, and D. D. Grimes, *Chem. Sci.* **9**, 6830 (2018).
- [31] R. Sawant, J. A. Blackmore, P. D. Gregory, J. Mur-Petit, D. Jaksch, J. Aldegunde, J. M. Hutson, M. R. Tarbutt, and S. L. Cornish, *New J. Phys.* **22**, 013027 (2020).
- [32] M. Hughes, M. D. Frye, R. Sawant, G. Bhole, J. A. Jones, S. L. Cornish, M. R. Tarbutt, J. M. Hutson, D. Jaksch, and J. Mur-Petit, *Phys. Rev. A* **101**, 062308 (2020).
- [33] K.-K. Ni, S. Ospelkaus, M. H. G. de Miranda, A. Pe'er, B. Neyenhuis, J. J. Zirbel, S. Kotochigova, P. S. Julienne, D. S. Jin, and J. Ye, *Science* **322**, 231 (2008).
- [34] J. G. Danzl, E. Haller, M. Gustavsson, M. J. Mark, R. Hart, N. Bouloufa, O. Dulieu, H. Ritsch, and H.-C. Nägerl, *Science* **321**, 1062 (2008).
- [35] F. Lang, K. Winkler, C. Strauss, R. Grimm, and J. Hecker Denschlag, *Phys. Rev. Lett.* **101**, 133005 (2008).
- [36] T. Takekoshi, L. Reichsöllner, A. Schindewolf, J. M. Hutson, C. R. Le Sueur, O. Dulieu, F. Ferlaino, R. Grimm, and H.-C. Nägerl, *Phys. Rev. Lett.* **113**, 205301 (2014).
- [37] P. K. Molony, P. D. Gregory, Z. Ji, B. Lu, M. P. Köppinger, C. R. Le Sueur, C. L. Blackley, J. M. Hutson, and S. L. Cornish, *Phys. Rev. Lett.* **113**, 255301 (2014).
- [38] J. W. Park, S. A. Will, and M. W. Zwielerlein, *Phys. Rev. Lett.* **114**, 205302 (2015).
- [39] M. Guo, B. Zhu, B. Lu, X. Ye, F. Wang, R. Vexiau, N. Bouloufa-Maafa, G. Quémener, O. Dulieu, and D. Wang, *Phys. Rev. Lett.* **116**, 205303 (2016).
- [40] T. M. Rvachov, H. Son, A. T. Sommer, S. Ebadi, J. J. Park, M. W. Zwielerlein, W. Ketterle, and A. O. Jamison, *Phys. Rev. Lett.* **119**, 143001 (2017).
- [41] F. Seeßelberg, N. Buchheim, Z.-K. Lu, T. Schneider, X.-Y. Luo, E. Tiemann, I. Bloch, and C. Gohle, *Phys. Rev. A* **97**, 013405 (2018).
- [42] H. Yang, D.-C. Zhang, L. Liu, Y.-X. Liu, J. Nan, B. Zhao, and J.-W. Pan, *Science* **363**, 261 (2019).
- [43] K. K. Voges, P. Gersema, M. Meyer zum Alten Borgloh, T. A. Schulze, T. Hartmann, A. Zenesini, and S. Ospelkaus, *Phys. Rev. Lett.* **125**, 083401 (2020).
- [44] E. S. Shuman, J. F. Barry, and D. DeMille, *Nature* **467**, 820 (2010).
- [45] J. F. Barry, D. J. McCarron, E. B. Norrgard, M. H. Steinecker, and D. DeMille, *Nature* **512**, 286 (2014).
- [46] S. Truppe, H. J. Williams, M. Hambach, L. Caldwell, N. J. Fitch, E. A. Hinds, B. E. Sauer, and M. R. Tarbutt, *Nat. Phys.* **13**, 1173 (2017).
- [47] I. Kozryyev, L. Baum, K. Matsuda, B. L. Augenbraun, L. Anderegg, A. P. Sedlack, and J. M. Doyle, *Phys. Rev. Lett.* **118**, 173201 (2017).
- [48] L. Anderegg, B. L. Augenbraun, Y. Bao, S. Burchesky, L. W. Cheuk, W. Ketterle, and J. M. Doyle, *Nat. Phys.* **14**, 890 (2018).
- [49] A. L. Collopy, S. Ding, Y. Wu, I. A. Finneran, L. Anderegg, B. L. Augenbraun, J. M. Doyle, and J. Ye, *Phys. Rev. Lett.* **121**, 213201 (2018).
- [50] S. Ospelkaus, K.-K. Ni, G. Quémener, B. Neyenhuis, D. Wang, M. H. G. de Miranda, J. L. Bohn, J. Ye, and D. S. Jin, *Phys. Rev. Lett.* **104**, 030402 (2010).
- [51] B. Yan, S. A. Moses, B. Gadway, J. P. Covey, K. R. Hazzard, A. M. Rey, D. S. Jin, and J. Ye, *Nature* **501**, 521 (2013).
- [52] P. D. Gregory, J. Aldegunde, J. M. Hutson, and S. L. Cornish, *Phys. Rev. A* **94**, 041403(R) (2016).
- [53] S. A. Will, J. W. Park, Z. Z. Yan, H. Loh, and M. W. Zwielerlein, *Phys. Rev. Lett.* **116**, 225306 (2016).
- [54] M. Guo, X. Ye, J. He, G. Quémener, and D. Wang, *Phys. Rev. A* **97**, 020501(R) (2018).
- [55] J. A. Blackmore, P. D. Gregory, S. L. Bromley, and S. L. Cornish, *Phys. Chem. Chem. Phys.* **22**, 27529 (2020).

- [56] A. V. Gorshkov, S. R. Manmana, G. Chen, J. Ye, E. Demler, M. D. Lukin, and A. M. Rey, *Phys. Rev. Lett.* **107**, 115301 (2011).
- [57] A. V. Gorshkov, S. R. Manmana, G. Chen, E. Demler, M. D. Lukin, and A. M. Rey, *Phys. Rev. A* **84**, 033619 (2011).
- [58] K. R. A. Hazzard, S. R. Manmana, M. Foss-Feig, and A. M. Rey, *Phys. Rev. Lett.* **110**, 075301 (2013).
- [59] S. A. Moses, J. P. Covey, M. T. Miecnikowski, B. Yan, B. Gadway, J. Ye, and D. S. Jin, *Science* **350**, 659 (2015).
- [60] L. Reichsöllner, A. Schindewolf, T. Takekoshi, R. Grimm, and H.-C. Nägerl, *Phys. Rev. Lett.* **118**, 073201 (2017).
- [61] L. R. Liu, J. D. Hood, Y. Yu, J. T. Zhang, K. Wang, Y.-W. Lin, T. Rosenband, and K.-K. Ni, *Phys. Rev. X* **9**, 021039 (2019).
- [62] L. Anderegg, L. W. Cheuk, Y. Bao, S. Burchesky, W. Ketterle, K.-K. Ni, and J. M. Doyle, *Science* **365**, 1156 (2019).
- [63] S. Kotochigova and E. Tiesinga, *Phys. Rev. A* **73**, 041405(R) (2006).
- [64] R. Vexiau, D. Borsalino, M. Lepers, A. Orbán, M. Aymar, O. Dulieu, and N. Bouloufa-Maafa, *Int. Rev. Phys. Chem.* **36**, 709 (2017).
- [65] M. Li, A. Petrov, C. Makrides, E. Tiesinga, and S. Kotochigova, *Phys. Rev. A* **95**, 063422 (2017).
- [66] F. Seeßelberg, X.-Y. Luo, M. Li, R. Bause, S. Kotochigova, I. Bloch, and C. Gohle, *Phys. Rev. Lett.* **121**, 253401 (2018).
- [67] B. Neyenhuis, B. Yan, S. A. Moses, J. P. Covey, A. Chotia, A. Petrov, S. Kotochigova, J. Ye, and D. S. Jin, *Phys. Rev. Lett.* **109**, 230403 (2012).
- [68] P. D. Gregory, J. A. Blackmore, J. Aldegunde, J. M. Hutson, and S. L. Cornish, *Phys. Rev. A* **96**, 021402(R) (2017).
- [69] J. A. Blackmore, L. Caldwell, P. D. Gregory, E. M. Bridge, R. Sawant, J. Aldegunde, J. Mur-Petit, D. Jaksch, J. M. Hutson, B. E. Sauer *et al.*, *Quantum Sci. Technol.* **4**, 014010 (2018).
- [70] S. Kotochigova and D. DeMille, *Phys. Rev. A* **82**, 063421 (2010).
- [71] H. Katori, M. Takamoto, V. G. Pal'chikov, and V. D. Ovsiannikov, *Phys. Rev. Lett.* **91**, 173005 (2003).
- [72] J. Ye, H. J. Kimble, and H. Katori, *Science* **320**, 1734 (2008).
- [73] S. S. Kondov, C. H. Lee, K. H. Leung, C. Liedl, I. Majewska, R. Moszynski, and T. Zelevinsky, *Nat. Phys.* **15**, 1118 (2019).
- [74] R. Bause, M. Li, A. Schindewolf, X.-Y. Chen, M. Duda, S. Kotochigova, I. Bloch, and X.-Y. Luo, *Phys. Rev. Lett.* **125**, 023201 (2020).
- [75] B. Sundar, B. Gadway, and K. R. Hazzard, *Sci. Rep.* **8**, 9236 (2018).
- [76] A. Petrov, C. Makrides, and S. Kotochigova, *Mol. Phys.* **111**, 1731 (2013).
- [77] J. Aldegunde, B. A. Rivington, P. S. Żuchowski, and J. M. Hutson, *Phys. Rev. A* **78**, 033434 (2008).
- [78] O. Docenko, M. Tamanis, R. Ferber, T. Bergeman, S. Kotochigova, A. V. Stolyarov, A. de Faria Nogueira, and C. E. Fellows, *Phys. Rev. A* **81**, 042511 (2010).
- [79] O. Docenko, M. Tamanis, R. Ferber, H. Knöckel, and E. Tiemann, *Phys. Rev. A* **83**, 052519 (2011).
- [80] M. Rakić, R. Beuc, N. Bouloufa-Maafa, O. Dulieu, R. Vexiau, G. Pichler, and H. Skenderović, *J. Chem. Phys.* **144**, 204310 (2016).
- [81] A. Chotia, B. Neyenhuis, S. A. Moses, B. Yan, J. P. Covey, M. Foss-Feig, A. M. Rey, D. S. Jin, and J. Ye, *Phys. Rev. Lett.* **108**, 080405 (2012).
- [82] T. Schuster, F. Flicker, M. Li, S. Kotochigova, J. E. Moore, J. Ye, and N. Y. Yao, [arXiv:1901.08597](https://arxiv.org/abs/1901.08597) [Phys. Rev. Lett. (to be published)].